Biochemical Sensing with an Arrayed Silicon Nanowire Platform

R. Ravindran, J. A. Sadie, K. E. Scarberry, H. S. Yang, M. S. Bakir, J. F. McDonald, and J. D. Meindl
Georgia Institute of Technology
791 Atlantic Dr. NW, Atlanta, GA 30332
rravindran@gatech.edu

Abstract

In this paper, we present our vision of a highly scalable arrayed biochemical sensor platform. This platform combines the advantages of refined and entrenched technologies like top-down integrated circuit fabrication and clinical assays with emerging technologies like three-dimensional stacking and label-free sensing. We demonstrate fabrication concepts and preliminary sensing results on ovarian cell lines prior to engaging in a discussion about relevant applications with regard to the exciting recent advances in genomics and oncology.

Background

As it currently stands, nearly all biological assays deployed in clinical settings rely on the use of labels. Most commonly, these labels are fluorophores. The use of such labels adds to the complexity and limitations of conventional assays in a number of ways. First, detection of the fluorophore requires an optical excitation source that would, at best, be inefficient if made in Si. Second, the labeling process itself introduces one or more processing steps. Third, the emission spectra of fluorophores, even quantum dots, are sufficiently wide that only a limited number can be delineated with certainty in any one test. [1] While methods employing labels do offer excellent sensitivity in applications ranging from confocal microscopy to immunoassays, they do not lend themselves to high-density, on-chip sensing.

The solution to this – one that has been explored with particular vigor over the past decade – is the use of label-free detection. [2, 3] A number of specific approaches are possible, but the general idea of label-free detection is to use a property inherent to the biomolecule to detect it directly after it has been specifically captured on or near the sensor without the use of additional labels. For the purposes of this paper, the biomolecule of interest will be referred to as the target. The target can posses many detectable properties, but most commonly, label-free sensing comes down to two in particular – mass and charge. In both cases, the target could be detected specifically at a sensor site through an interaction such as that between an antigen and antibody or complementary single stranded nucleic acid sequences, or it can be detected non-specifically. This paper implements the later.

There are several variations of mass-based sensors, but typically the mass of the captured target molecule results in the deflection of a cantilever, the alteration of a propagating acoustic wave, or a change in oscillator resonance properties. [4] Charge-based sensors typically fall into devices that are field effect based, where the charge of a captured target modulates the current through the channel of a semiconductor. [2, 3] In our work, we use a silicon nanowire (SiNW) charge-based sensor, largely due to how well it lends itself to top-down IC fabrication and the simplicity of a DC biased, three-terminal measurement setup.

While simply using SiNW sensors, or any other label-free scheme in isolation does leverage the advantage of simplicity compared to labeled schemes, there is a far more substantial advantage to be had in the simultaneous detection of tens, hundreds, or even thousands of biochemical targets [2, 5] on a chip fabricated using a workflow that is harmonious with IC fabrication methods like non-planar CMOS and three-dimensional stacking (3DS). Essentially, this amounts to a modern, label-free, high-density, and electronic interpretation of the ubiquitous and five decade old microliter plate. The general principles of simplicity, scalability, manufacturability, and clinical relevance guide the ideas touched upon in the following sections. There will no doubt be a significant demand for devices with such capabilities as personalized medicine comes to realization.

This paper is divided into four sections. The first section describes the fabrication of a SiNW array with 16 sensors in isolated polymer wells. The second demonstrates a practical use of this sensor array for a new type of ovarian cancer identification. The third summarizes our development and integration of 3DS technologies that are fully compatible with such a sensor array and that can enable significant scalability. The fourth and final section is a discussion of future extensions and promising applications.

Silicon Nanowire Array Fabrication

The SiNW array fabrication process is top-down and CMOS compatible from start to finish. It begins with a silicon-on-insulator (SOI) wafer with a 70 nm thick device layer (p-type, 1-10 Ω-cm) and a 145 nm buried oxide (BOX) layer. E-beam lithography (EBL) is used to define a 4 x 4 array of 50 nm wide x 70 nm tall x 50 μm long SiNWs per 1 x 1 cm chip. It is important to note that this relatively low density of sensors is chosen not because of any inherent process or design limitations, but to facilitate simple manual sample loading via micropipettes for the tests reported in this paper. We suggest realistically achievable densities in the future extensions section. Following EBL, the device layer is anisotropically etched down to the BOX using an Ar/Cl_2 plasma in an ICP, in turn forming the SiNWs. The sample then undergoes a 900 ˚C RTP anneal in an O_2 ambient to reduce etch damage and grow a thin field oxide. Optical lithography is then used to define Al source and drain electrodes which are subsequently deposited using e-beam evaporation. After lift-off, a 450 ˚C RTP anneal in forming gas creates ohmic contacts between the Al electrodes and SiNWs. To protect the electrodes and define the wells, two layers of SU-8 are deposited. The first 2 μm thick layer protects the electrodes and opens 40 x 40 μm windows around the SiNWs and the probing pads while the second 100

978-1-4244-6412-8/10/$26.00 ©2010 IEEE

µm thick layer forms the 1 mm diameter wells into which the samples are loaded. An overview of this workflow is shown in Figure 1 and images of a completed SiNW array in Figure 2.

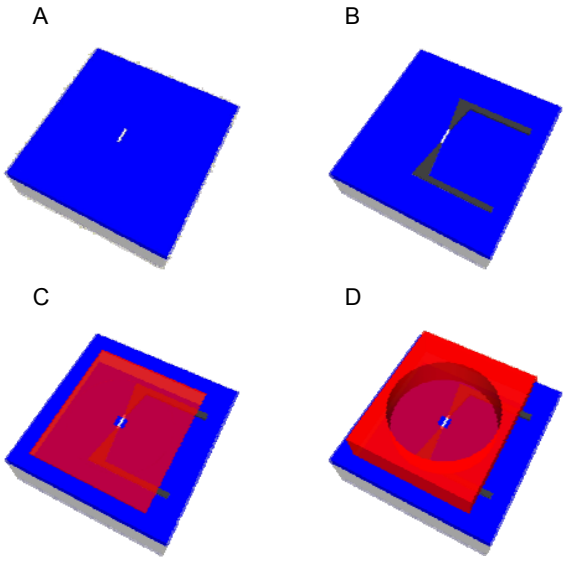

Figure 1: A simplified schematic of the fabrication process. A SiNW is patterned and etched (A), electrodes are patterned and deposited (B), the first SU-8 layer is deposited and patterned to protect the Al electrodes (C), and the second SU-8 layer is deposited and patterned to define the wells (D). Light grey is Si, blue is the BOX, dark grey is the Al, and red is the SU-8.

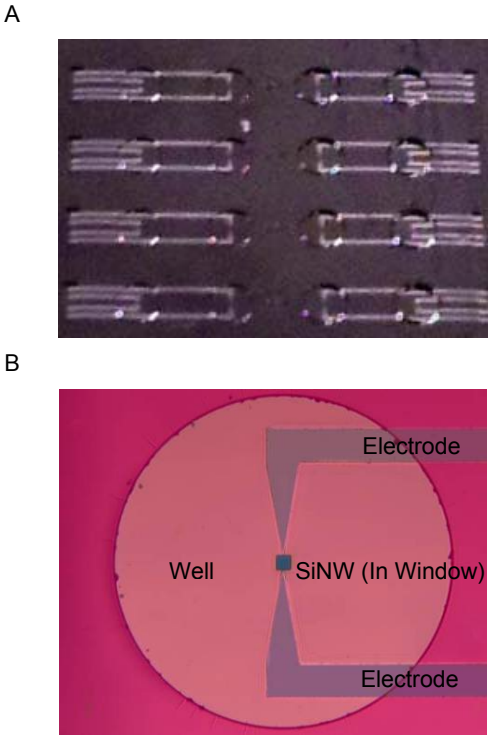

Figure 2: Optical images of a complete 4 x 4 SiNW array constituting a single chip (A) and an individual well (B).

The devices are operated as accumulation mode back-gated transistors in the linear region with all sensors on the chip first characterized under dry conditions. During this characterization, both the I_D vs. V_{DS} and I_D vs. V_{GS} curves are measured. The latter (not shown) is used to determine the peak transconductance point V_{DS} = -2 V and this bias point is then used for all subsequent wet sensing measurements. The peak back-gated transconductance is typically in the 0.1 µS range and occurs between V_{GS} = -15 to -20 V. All measurements were performed using a HP 4156A semiconductor analyzer.

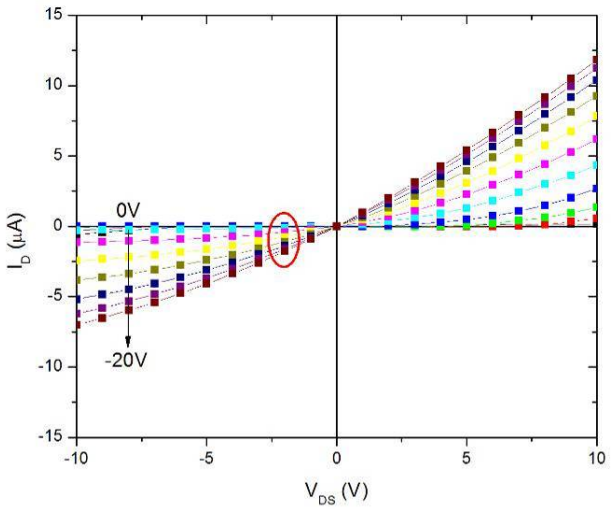

Figure 3: Standard I_D vs. V_{DS} curves for back-gate voltages from V_{GS} = 0 to -20 V. The red circle indicates the V_{DS} = -2 V point at which the devices are operated for sensing measurements.

Arrayed Cancer Cell Sensing

There are a number of uses for a high-density sensor array in a clinical or research setting. Some of these will be discussed in the future extensions section. However we choose a rather simple application – verification of the response to identical samples across multiple tests – for our initial use. It should be pointed out that there is a noteworthy reason for running a series of verification tests as opposed to testing different samples or attempting to sense different targets. The particular test we show in this paper for differentiating between healthy and cancerous cells has not been previously implemented. Here, verification is a worthwhile and pragmatic use of a label-free sensor array.

For preliminary device characterization in biologically relevant solutions, a test sensor is first used to perform pH sensing, one of the canonical tests of charge-based sensors. The relative concentration of H^+ and OH^- ions in a buffer solution results in the protonation or deprotonation of the terminal Si–OH groups, thereby altering the surface potential on the SiNW and consequently the channel conductance. We used phosphate buffered saline (PBS) at pH values of 2.8, 7.6, and 12.3. Figure 4 shows the response of a SiNW sensor to these three buffers. As expected, the more basic pH 12.8 buffer with an abundance of negatively charged OH^- ions increases the magnitude of the drain current. Conversely, the more acidic pH 2.8 buffer with an abundance of positively

charged H^+ ions decreases the magnitude of the drain current. For all tests in this section a micropipette is used to both introduce and withdraw ~10 µL of solution contained in the hydrophobic SU-8 wells. The micropipette tips were changed between solutions. Also, the t = 0 point starts after ~100 s of stabilization time (not shown) after the first sample has been introduced into the well.

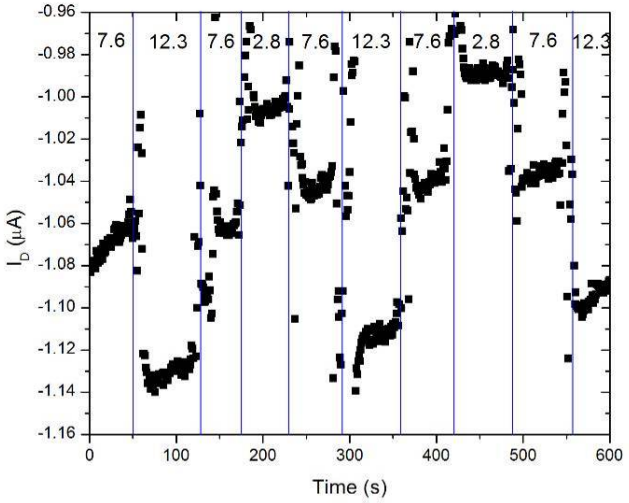

Figure 4: I_D vs. time for PBS at three different pH values on a test SiNW sensor. The PBS solutions are at pH values of 2.8, 7.6, and 12.3.

Naturally, the objective here is not to recreate a pH meter, but rather to validate the merits of our SiNW array in a biochemical sensing application. To this end, we developed a new method for differentiating between two human ovarian cell lines. The first of these, IOSE, is an immortalized cell line that represents healthy epithelial ovarian cells. The second, HEY, is a cell line that represents cancerous epithelial ovarian cells. Working under the hypothesis that the contents and makeup of the two cell lines should differ due to the more aggressive proliferation demands of the HEY cells, we make samples containing the contents of these cells at specific concentrations. At the highest concentration, two samples are made, each with the contents of 750,000 cells from either the IOSE or HEY cell lines per 1 mL of pH 7.6 PBS. These two samples are then serially diluted into concentrations of 75,000 cells/mL PBS and 7,500 cells/mL PBS.

Five sensors from a single 4 x 4 array are then used to run identical tests. The tests consist of switching between the HEY and IOSE samples at all three concentrations. Each sample is left on the chip for approximately 100 s. A time-dependent plot from one of these five tests is shown in Figure 5.

A number of observations can be made from these tests. The I_D magnitude is greater for the HEY sample than it is for the IOSE sample. We do not expect the pH value of the buffered solutions to be notably different. Thus, the change in current is not occurring because of the protonation or deprotonation of the Si-OH groups on the SiNW field oxide as was the case in the pH tests. We know that the HEY sample must contain more negative charge (or less positive charge) than the IOSE because of the larger HEY I_D magnitude. A plausible explanation is differences in the intracellular ion concentrations between the two cell lines. This is supported by the fact that a number of positively charged metal ions have been reported to be found in lower concentrations in certain cancer cells as compared to their healthy equivalents. [6] Unlike the pH testing, the ions in the HEY and IOSE solutions are not expected to directly interact with the Si-OH surface groups on the field oxide. The likely explanation is that the modulation arises simply through the close proximity of ionic charges in the solution to the conducting channel in the SiNW. One indication of this is that the signal to noise ratio (defined as μ/σ) is roughly three times worse for the cancer cell tests than the pH tests.

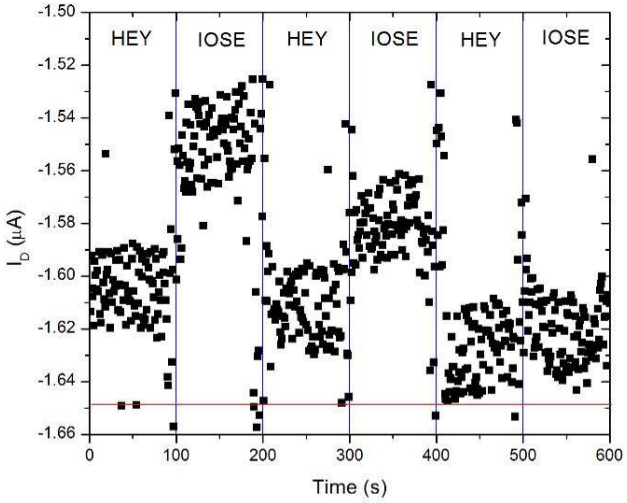

Figure 5: I_D vs. time for samples derived from the two different cell lines in three different concentrations. In order from left to right, the cell lines and concentrations are 750,000 HEY cells/mL, 750,000 IOSE cells/mL 75,000 HEY cells/mL, 75,000 IOSE cells/mL 7,500 HEY cells/mL, and 7,500 IOSE cells/mL. The red line indicates the average baseline I_D value of pure PBS.

The relative differences in the HEY and IOSE currents for all three concentrations and all five tests are shown below.

To confirm the statistical significance of the difference between the HEY and IOSE current values, we run a two-tailed, unpaired t-test on all the tests to obtain the associated p-values. To avoid noise associated with the sample exchanges, only I_D values from the middle 50 s for each sample are used. From this data, we conclude that down to a concentration of 75,000 cells/mL, all five sensors yield statistically significant ($p < 0.05$) results. The following table lists the p-values.

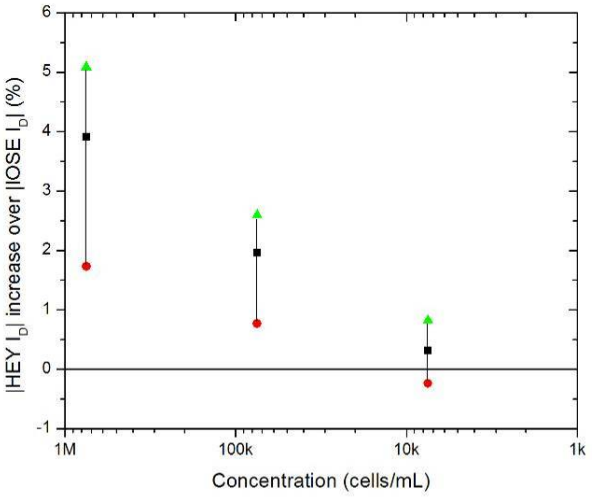

Figure 6: The increase in the magnitude of the HEY I_D relative to the IOSE I_D expressed as a percentage. The data shown is from tests on five distinct sensors on a single chip at three concentrations (750,000 cells/mL, 75,000 cells/mL, and 7,500 cells/mL) per test. The black squares indicate the mean, the red circles the minimum, and the green triangles the maximum.

	Sensor				
cells/mL	1	2	3	4	5
750,000	< .001	< .001	< .001	< .001	< .001
75,000	< .001	< .001	< .001	< .001	< .001
7,500	0.216	< .001	0.059	0.021	0.010

Table 1: P-values for the five sensors tested at each of the three different concentrations.

Interestingly, in Figure 6 we see a log-linear relationship between the cell concentration and change in current. Such behavior has been previously reported for isolated and purified cancer markers like prostate specific antigen. [7] However, with no previously reported field-effect sensor data on detecting targets from live cancer cells, we do not have a definitive answer to explain this behavior. There is also the possibility that our sensor would not show notably greater differences in the HEY and IOSE currents at concentrations much higher than 750,000 cells/mL. In fact, preliminary testing at higher concentrations suggests that this is likely the case.

One of the motivating factors for applying this new method of cell identification is to show the power of a top-down fabricated sensor array. While our tests here use identical samples at different concentrations for the purposes of studying the variability and sensitivity limits of our sensor array, it is rather straightforward to imagine scenarios where hundreds or thousands of different tests are conducted simultaneously in a commercially fabricated SiNW array. A remarkable number of disease markers could potentially be screened for and an abundance of statistical data gathered from a single chip.

Three-Dimensional Stacking

There are several issues that limit high-density sensor arrays. First, and most importantly, is the dichotomy between liquid samples and electronic components. Second, many thousands of sensors, each detecting a different target from a sample, might need to be accessed simultaneously. This would render row and column based access schemes such as that used for memories impractical. Routing electrodes for each sensor to the chip edge would also be needlessly space consuming and hinder how well the density of an array would scale with the number of sensors on a chip. Further, for most research and clinical applications, it would be desirable to have a disposable chip to avoid contamination – much as is currently the case with microliter plates. In this section we discuss complementary work we have carried out in parallel with sensor array development to address these requirements.

One part of the solution is to use through silicon vias (TSVs) to electrically connect the sensor array side to the backside. We implement this by extending the process reported in Ref. 8. The process begins by depositing a 2 µm thick PECVD SiO_2 layer on the device Si of a pristine SOI wafer. Then we use an ICP Bosch process to etch 100 µm diameter vias from the handle wafer side, stopping at the PECVD oxide on the device Si side. These TSVs are located where the Al electrodes will end. The sidewalls of the TSVs are passivated from the backside with another PECVD SiO_2 layer. The oxide on the device side is then patterned into a mesh over the vias and removed from all other areas, revealing once more the pristine device Si layer. We then proceed as described previously with sensor array fabrication. After completing the sensor array, we electroplate Cu into the vias to connect the Al electrodes on the sensor side to solder bumps on the backside. TSV fabrication details specific to our sensor array can be found in Ref. 9. A depiction of this process is shown in Figure 7 and an image of TSVs integrated with a sensor array chip in Figure 8.

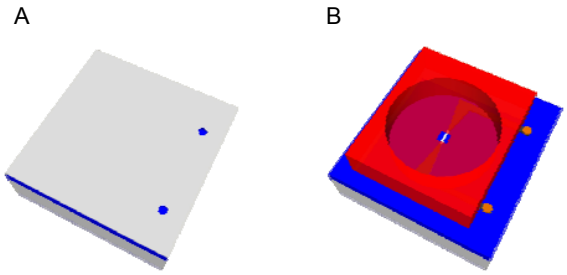

Figure 7: Another simplified schematic, this time depicting the integration of TSVs with the sensor array. It begins with first etching the TSV, passivating the sidewalls with oxide, and patterning the oxide mesh mask on a SOI wafer (A). Then sensor fabrication is completed as depicted previously in Figure 1. Finally Cu is electroplated into the TSVs to connect the Al electrodes to solder bumps on the backside (B). Here again, light grey is Si, blue is oxide, dark grey is the Al, and red is the SU-8.

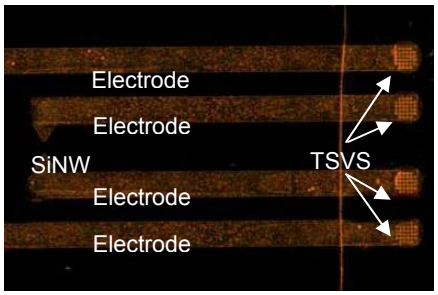

Figure 8: Optical image of TSVs at the ends of two pairs electrodes on a sensor array chip.

Unfortunately, time constraints prevented us from repeating the biochemical sensing measurements on a chip with TSVs. However, preliminary testing of isolated TSVs has indicated low resistances (<< 1 Ω) and negligible leakage through the passivating oxide on the sidewalls at typical measurement biases – both indicators that the successful integration of TSVs with our sensor array should not face unsolvable challenges.

Another part of the solution lies in the use of high-density mechanically flexible (compliant) interconnects to enable a simple interface between the backside of a sensor chip and the processing circuitry needed for signal conditioning and measurement. A detailed discussion of our work on compliant interconnects with a unique and suitable three-dimensional topology can be again be found in Ref. 9. We have fabricated these interconnects at pitches down to 50 µm and vertical displacements greater than 20 µm. Ultimately, the goal is to use these compliant interconnects to electrically connect the solder bumps on the backside of disposable sensor chips with a reusable electronic measurement setup.

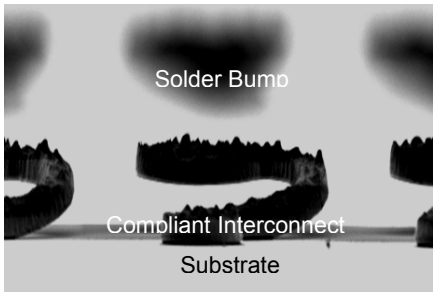

Figure 9: SEM image of compliant interconnects.

To summarize, TSVs would be used to connect individual SiNW sensors on the device side of an SOI based disposable chip to solder bumps on the backside. Compliant interconnects would connect these solder bumps to the electronic measurement circuitry. This is depicted below.

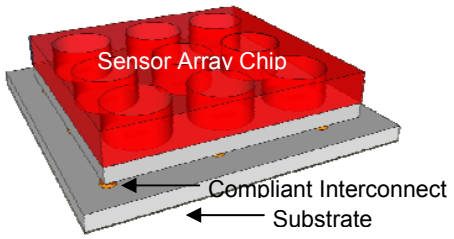

Figure 10: Schematic of a sensor chip (in this case a 3 x 3 array) connected via compliant interconnects to a substrate containing the reusable electronic measurement setup.

Future Extensions

To repeat the theme of this paper, our goal is to develop a disposable high-density label-free sensor array chip. While a number of methodologies, some of which have been discussed in this paper, and all of which are feasible using contemporary manufacturing processes need to come together to realize this, it is a worthwhile exercise to discuss some potential applications. It is also notable that while we use SiNWs as our label-free sensor of choice, nearly all the components of the platform are sensor agnostic and could work equally well with mass based and optical sensors.

We previously mentioned that our relatively low-density array was simply to facilitate manual sample loading. Even at our modest fabrication dimensions, each sensor site combined with the source and drain TSVs (neglecting the electrode length, which can be shortened) only occupies a 240 x 100 µm area. If we generously allocate 500 x 500 µm per sensor site, 400 sensors could be fabricated on a 1 x 1 cm chip. With scaling, thousands of sensors could be fabricated in the same area. Naturally, this would require automated fluid handling systems which already exist. However, this opens the door for many types of new assays.

We predict that most of these assays will deal with disease marker identification and in particular, over expressed proteins. With the development of rapid and low-cost DNA sequencing, we do not anticipate this sensor platform finding use in gene sequencing. [10] Rather, we believe it will be used for identifying early stage disease markers such as those for heart disease and cancer. Large numbers of markers for various diseases have been identified in recent years. [5, 11] However dozens of markers often have to be screened to identify individual diseases with specificity while avoiding false positives and negatives. A high-density biochemical sensor array provides an excellent opportunity to make early-stage screening for tens or hundreds of complex diseases such as various cancers as routine as a common lipid profile.

Conclusions

This paper laid out our vision for a modern label-free biochemical sensing platform. We demonstrated the top-down fabrication of a SiNW sensor array and its use in a new method for differentiating between healthy and cancerous cells. We then discussed our preliminary work on stacking methods that will ultimately enable disposable and high-density chips as well as future applications. The theme throughout has been one of how to provide biologists and

clinicians with a modern tool, as interpreted through IC manufacturing, to complement the notable recent and emerging advances in linking diseases and characteristic biochemical markers.

Acknowledgments

The authors thank Dr. Nelly Auersperg for access to the Canadian Ovarian Tissue Bank. R. Ravindran acknowledges support received through the IBSI Graduate Fellowship.

References

1. Han, M. *et al.*, "Quantum-dot-tagged microbeads for multiplexed optical coding of biomolecules," *Nature Biotechnology*, Vol. 19, (2001), pp. 631-635.
2. Zheng, G. *et al.*, "Multiplexed electrical detection of cancer markers with nanowire sensor arrays," *Nature Biotechnology*, Vol. 23, (2005), pp. 1294-1301.
3. Stern, E. *et al.*, "Label-free immunodetection with CMOS-compatible semiconducting nanowires," *Nature*, Vol. 445, (2007), pp. 519-522.
4. Braun, T. *et al.*, "Quantitative time-resolved measurement of membrane protein-ligand interactions using microcantilever array sensors," *Nature Nanotechnology*, Vol. 4, (2008), pp. 179-185.
5. Wulfkuhle, J. D. *et al.*, "Proteomic Applicatons for the Early Detection of Cancer," *Nature Cancer*, Vol. 3, (2003), pp. 267-275.
6. Ling, G. N. *et al.*, "Low Paramagnetic-Ion Content in Cancer Cells: Its Signficance in Cancer Detection by Magnetic Resonance Imaging," *Physiological Chemistry & Physics & Medical NMR*, Vol. 22, (1990), pp. 1-14.
7. Kim, A. *et al.*, "Ultrasensitive, label-free, and real-time immunodetection using silicon field-effect transistors," *Applied Physics Letters*, Vol. 91, (2007), p. 103901.
8. Lai, J.-H. *et al.*, "A 'mesh' seed layer for improved through-silicon-via fabrication," *Journal of Micromechanics and Microengineering*, Vol. 20, (2010), p. 025016
9. Yang, H. S. *et al.*, To be published in the *Proceedings of the 60th Electronic Components and Technology Conference*, Las Vegas, NV, June, 2010
10. Pushkarev, D. *et al.*, "Single-molecule sequencing of an individual human genome," *Nature Biotechnology*, Vol. 27, (2009), pp. 847-850.
11. Pai, J. K. *et al.*, "Inflammatory Markers and the Risk of Cornonary Heart Disease in Men and Women," *The New England Journal of Medicine*, Vol. 351, (2004), pp. 2599-2610